7 The Electronic Bandstructure of Solids

Despite the success of the free-electron-gas model in describing electrons in crystals (Chap. 6), it must be recognized that the assumptions of the one-electron approximation and of a square-well potential, are oversimplifications. Thus one cannot expect this model to explain, for example, the fundamentally important optical and electronic properties of semiconductors. If one imagines, as discussed briefly in Chap. 1, that a solid is created by allowing initially free atoms to gradually approach one another, then the discrete nature of the energy levels of the isolated atoms should clearly be reflected in the properties of the solid. Indeed, discrete energy levels must be present in order to explain, e.g., the sharp resonance-like structures observed in the optical spectra of solids. An explanation of such features is beyond the scope of the free-electron-gas model. Furthermore, this model is unable to shed any light on the nature of semiconductors and insulators. To make further progress one has to take into account that the electronic states in solids form so-called bands. One can think of these as deriving from the states of the free atom.

In our present approximation, all deviations from perfect periodicity, be they static perturbations of the lattice or dynamic vibrations of the atoms, will be neglected. The assumption of an infinitely extended potential also means the neglect of all surface effects. To arrive at a finite crystal, i.e., one with a finite number of degrees of freedom, that is compatible with the infinite periodicity, one again makes use of the periodic boundary conditions introduced in Sect. 5.1.

7.1 General Symmetry Properties

We are now faced with the task of solving the time-independent Schrödinger equation for a single electron under the assumption that the potential $V(\boldsymbol{r})$ is periodic:

$$\mathscr{H}\psi(\boldsymbol{r}) = \left[-\frac{\hbar^2}{2m}\nabla^2 + V(\boldsymbol{r})\right]\psi(\boldsymbol{r}) = E\psi(\boldsymbol{r}) \,, \tag{7.1}$$

where

$$V(\boldsymbol{r}) = V(\boldsymbol{r} + \boldsymbol{r_n}); \quad \boldsymbol{r_n} = n_1\boldsymbol{a}_1 + n_2\boldsymbol{a}_2 + n_3\boldsymbol{a}_3 \,. \tag{7.2}$$

H. Ibach, H. Lüth, *Solid-State Physics*, 4th ed.,
DOI 10.1007/978-3-540-93804-0_7, © Springer-Verlag Berlin Heidelberg 2009

As in Sect. 3.2, $\boldsymbol{r_n}$ represents an arbitrary translation vector of the three-dimensional periodic lattice, i.e., $\boldsymbol{r_n}$ consists of multiples (n_1, n_2, n_3) of the three basis vectors $\boldsymbol{a}_1, \boldsymbol{a}_2, \boldsymbol{a}_3$ of the real-space lattice.

Since the potential $V(\boldsymbol{r})$ has the same periodicity as the lattice, it can be expanded in the following Fourier series:

$$V(\boldsymbol{r}) = \sum_{\boldsymbol{G}} V_{\boldsymbol{G}} \, \mathrm{e}^{\mathrm{i}\boldsymbol{G}\cdot\boldsymbol{r}} \, , \tag{7.3}$$

where the vector $\boldsymbol{G}$ must be a reciprocal lattice vector

$$\boldsymbol{G} = h\boldsymbol{g}_1 + k\boldsymbol{g}_2 + l\boldsymbol{g}_3 \, , \quad h, k, l \text{ integers.} \tag{7.4}$$

(in the one-dimensional case $\boldsymbol{G} \to G = h\,2\pi/a$). The most general plane-wave expansion of the required wavefunction $\psi(\boldsymbol{r})$ is

$$\psi(\boldsymbol{r}) = \sum_{\boldsymbol{k}} C_{\boldsymbol{k}} \, \mathrm{e}^{\mathrm{i}\boldsymbol{k}\cdot\boldsymbol{r}} \, . \tag{7.5}$$

Here $\boldsymbol{k}$ is a point in reciprocal space that is compatible with the periodic boundary conditions (Sects. 5.1 and 6.1). Substituting the expansions (7.3) and (7.5) into the Schrödinger equation (7.1) we obtain:

$$\sum_{\boldsymbol{k}} \frac{\hbar^2 k^2}{2m} C_{\boldsymbol{k}} \mathrm{e}^{\mathrm{i}\boldsymbol{k}\cdot\boldsymbol{r}} + \sum_{\boldsymbol{k}'\boldsymbol{G}} C_{\boldsymbol{k}'} V_{\boldsymbol{G}} \, \mathrm{e}^{\mathrm{i}(\boldsymbol{k}'+\boldsymbol{G})\cdot\boldsymbol{r}} = E \sum_{\boldsymbol{k}} C_{\boldsymbol{k}} \, \mathrm{e}^{\mathrm{i}\boldsymbol{k}\cdot\boldsymbol{r}} \, . \tag{7.6}$$

After renaming the summation indices this becomes

$$\sum_{\boldsymbol{k}} \mathrm{e}^{\mathrm{i}\boldsymbol{k}\cdot\boldsymbol{r}} \left[\left(\frac{\hbar^2 k^2}{2m} - E \right) C_{\boldsymbol{k}} + \sum_{\boldsymbol{G}} V_{\boldsymbol{G}} C_{\boldsymbol{k}-\boldsymbol{G}} \right] = 0 \, . \tag{7.7}$$

Since this condition is valid for every position vector $\boldsymbol{r}$, the expression in brackets, which is independent of $\boldsymbol{r}$, must vanish for every $\boldsymbol{k}$, i.e.,

$$\left(\frac{\hbar^2 k^2}{2m} - E \right) C_k + \sum_{\boldsymbol{G}} V_{\boldsymbol{G}} C_{\boldsymbol{k}-\boldsymbol{G}} = 0 \, . \tag{7.8}$$

This set of algebraic equations, which is simply a representation of the Schrödinger equation (7.1) in reciprocal space, couples only those expansion coefficients $C_{\boldsymbol{k}}$ of $\psi(\boldsymbol{r})$ (7.5), whose $\boldsymbol{k}$-values differ from one another by a reciprocal lattice vector $\boldsymbol{G}$. Thus $C_{\boldsymbol{k}}$ is coupled to $C_{\boldsymbol{k}-\boldsymbol{G}}$, $C_{\boldsymbol{k}-\boldsymbol{G}'}$, $C_{\boldsymbol{k}-\boldsymbol{G}''}$, … .

The original problem thus separates into N problems (N = number of unit cells), each corresponding to a $\boldsymbol{k}$-vector in the unit cell of the reciprocal lattice. Each of the N systems of equations yields a solution that can be represented as a superposition of plane waves whose wave vectors $\boldsymbol{k}$ differ only by reciprocal lattice vectors $\boldsymbol{G}$. The eigenvalues E of the Schrödinger equation (7.1) can thus be indexed according to $E_{\boldsymbol{k}} = E(\boldsymbol{k})$, and the wavefunction belonging to $E_{\boldsymbol{k}}$ is

$$\psi_{\boldsymbol{k}}(\boldsymbol{r}) = \sum_{\boldsymbol{G}} C_{\boldsymbol{k}-\boldsymbol{G}}\, \mathrm{e}^{\mathrm{i}(\boldsymbol{k}-\boldsymbol{G})\cdot\boldsymbol{r}} \tag{7.9}$$

or

$$\psi_{\boldsymbol{k}}(\boldsymbol{r}) = \sum_{\boldsymbol{G}} C_{\boldsymbol{k}-\boldsymbol{G}}\, \mathrm{e}^{-\mathrm{i}\boldsymbol{G}\cdot\boldsymbol{r}}\, \mathrm{e}^{\mathrm{i}\boldsymbol{k}\cdot\boldsymbol{r}} = u_{\boldsymbol{k}}(\boldsymbol{r})\, \mathrm{e}^{\mathrm{i}\boldsymbol{k}\cdot\boldsymbol{r}}\,. \tag{7.10 a}$$

The function $u_{\boldsymbol{k}}(\boldsymbol{r})$ introduced here is a Fourier series over reciprocal lattice points $\boldsymbol{G}$ and thus has the periodicity of the lattice. The wave vector $\boldsymbol{k}$, which, for periodic boundary conditions, can take the values (Sect. 6.1)

$$\begin{aligned} k_x &= 0,\ \pm 2\pi/L,\ \pm 4\pi/L, \ldots,\ \pm 2\pi n_x/L \\ k_y &= 0,\ \pm 2\pi/L,\ \pm 4\pi/L, \ldots,\ \pm 2\pi n_y/L \\ k_z &= 0,\ \pm 2\pi/L,\ \pm 4\pi/L, \ldots,\ \pm 2\pi n_z/L \end{aligned} \tag{7.10 b}$$

(L = macroscopic dimension of the crystal), yields the correct quantum numbers k_x, k_y, k_z or n_x, n_y, n_z, according to which the energy eigenvalues and quantum states may be indexed. In other words, we have shown that the solution of the one-electron Schrödinger equation for a periodic potential can be written as a modulated plane wave

$$\psi_{\boldsymbol{k}}(\boldsymbol{r}) = u_{\boldsymbol{k}}(\boldsymbol{r})\, \mathrm{e}^{\mathrm{i}\boldsymbol{k}\cdot\boldsymbol{r}} \tag{7.10 c}$$

with a modulation function

$$u_{\boldsymbol{k}}(\boldsymbol{r}) = u_{\boldsymbol{k}}(\boldsymbol{r} + \boldsymbol{r}_{\boldsymbol{n}}) \tag{7.10 d}$$

that has the periodicity of the lattice. This result is known as *Bloch's theorem*, and the wavefunctions given in (7.10 a–d) are called the *Bloch waves* or Bloch states of an electron (Fig. 7.1).

The strict periodicity of the lattice potential has further consequences that follow directly from the properties of the Bloch states. From the general representation of a Bloch wave (7.10 a), and by renaming the reciprocal lattice vectors $\boldsymbol{G}'' = \boldsymbol{G}' - \boldsymbol{G}$, it follows that

$$\begin{aligned} \psi_{\boldsymbol{k}+\boldsymbol{G}}(\boldsymbol{r}) &= \sum_{\boldsymbol{G}'} C_{\boldsymbol{k}+\boldsymbol{G}-\boldsymbol{G}'}\, \mathrm{e}^{-\mathrm{i}\boldsymbol{G}'\cdot\boldsymbol{r}}\, \mathrm{e}^{\mathrm{i}(\boldsymbol{k}+\boldsymbol{G})\cdot\boldsymbol{r}} \\ &= \left(\sum_{\boldsymbol{G}''} C_{\boldsymbol{k}-\boldsymbol{G}''}\, \mathrm{e}^{-\mathrm{i}\boldsymbol{G}''\cdot\boldsymbol{r}} \right) \mathrm{e}^{\mathrm{i}\boldsymbol{k}\cdot\boldsymbol{r}} = \psi_{\boldsymbol{k}}(\boldsymbol{r})\,, \end{aligned} \tag{7.11 a}$$

i.e.

$$\psi_{\boldsymbol{k}+\boldsymbol{G}}(\boldsymbol{r}) = \psi_{\boldsymbol{k}}(\boldsymbol{r})\,. \tag{7.11 b}$$

Thus Bloch waves whose wave vectors differ by a reciprocal lattice vector are identical. The Schrödinger equation (7.1):

$$\mathscr{H}\,\psi_{\boldsymbol{k}} = E(\boldsymbol{k})\,\psi_{\boldsymbol{k}} \tag{7.12}$$

and that for the same problem displaced by $\boldsymbol{G}$:

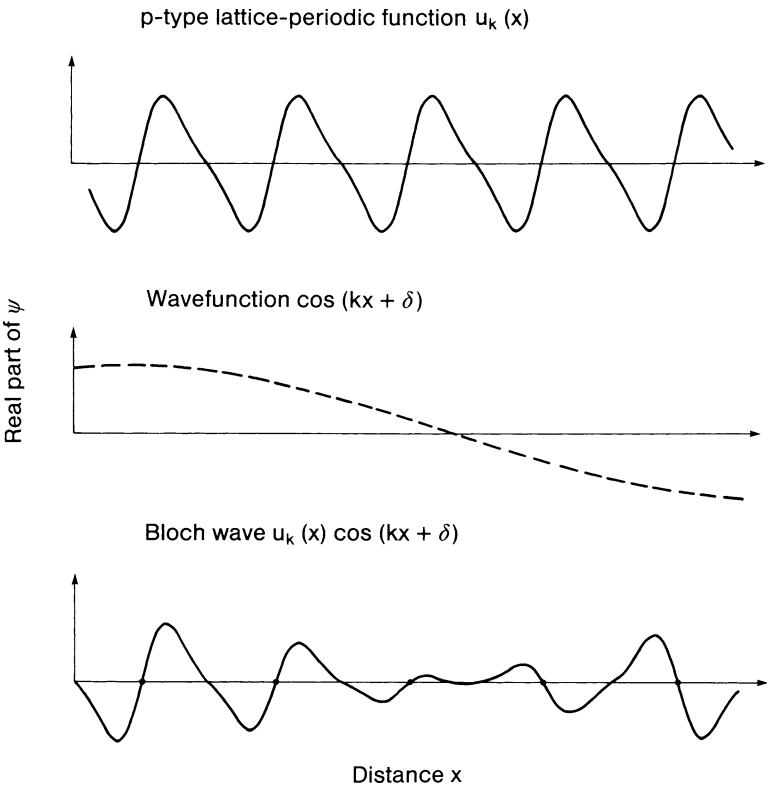

Fig. 7.1. Example of the construction of a Bloch wave $\psi_{\boldsymbol{k}}(\boldsymbol{r}) = u_{\boldsymbol{k}}(\boldsymbol{r})\mathrm{e}^{\mathrm{i}\boldsymbol{k}\cdot\boldsymbol{r}}$ from a lattice-periodic function $u_{\boldsymbol{k}}(\boldsymbol{r})$ with p-type bonding character and a plane wave

$$\mathscr{H}\psi_{\boldsymbol{k}+\boldsymbol{G}} = E(\boldsymbol{k}+\boldsymbol{G})\psi_{\boldsymbol{k}+\boldsymbol{G}} \tag{7.13}$$

together with (7.11 b) then yield

$$\mathscr{H}\psi_{\boldsymbol{k}} = E(\boldsymbol{k}+\boldsymbol{G})\psi_{\boldsymbol{k}} \,. \tag{7.14}$$

Comparing (7.12) with (7.14) we see that

$$E(\boldsymbol{k}) = E(\boldsymbol{k}+\boldsymbol{G}) \,. \tag{7.15}$$

Thus the energy eigenvalues $E(\boldsymbol{k})$ are a periodic function of the quantum numbers $\boldsymbol{k}$, i.e., of the wave vectors of the Bloch waves.

Similar to the case of phonons, whose $\omega(\boldsymbol{q})$ can be described by dispersion surfaces in reciprocal $\boldsymbol{q}$-space, the one-electron states of a periodic potential can be represented by energy surfaces $E = E(\boldsymbol{k})$ that are a periodic function of the wave vector (quantum number) in reciprocal $\boldsymbol{k}$-space. Taken together, these energy surfaces form the *electronic bandstructure* of the crystal. Since both $\psi_{\boldsymbol{k}}(\boldsymbol{r})$ and $E(\boldsymbol{k})$ are periodic in reciprocal space, one only needs to know these functions for $\boldsymbol{k}$-values in the first Brillouin zone

(Sect. 3.5). A periodic continuation of the functions then provides the values throughout the whole of $\boldsymbol{k}$-space.

7.2 The Nearly Free-Electron Approximation

To understand the general concept of electronic bands it is particularly instructive to consider the limiting case of a vanishingly small periodic potential. We therefore imagine that the periodic potential starts at zero and is gradually"switched on". What happens then to the energy states of the free electrons which, in the square-well potential, were described by the energy parabola $E = \hbar^2 k^2/2m$? In the extreme case where the potential is still zero, i.e., where all Fourier coefficients $V_{\boldsymbol{G}}$ (7.3) vanish, one must nonetheless consider the symmetry requirements of the periodicity, since the requirements will be a decisive factor even for the smallest nonvanishing potential. This general demand of periodicity immediately implies, from (7.15), that the possible electron states are not restricted to a single parabola in $\boldsymbol{k}$-space, but can be found equally well on parabolas shifted by any $\boldsymbol{G}$-vector:

$$E(\boldsymbol{k}) = E(\boldsymbol{k} + \boldsymbol{G}) = \frac{\hbar^2}{2m} |\boldsymbol{k} + \boldsymbol{G}|^2 \,. \tag{7.16}$$

For the one-dimensional case ($\boldsymbol{G} \to G = h2\pi/a$) this is depicted in Fig. 7.2.

Since the behavior of $E(\boldsymbol{k})$ is periodic in $\boldsymbol{k}$-space, it is sufficient to represent this in the first Brillouin zone only. To achieve this one simply displaces the part of the parabola of interest by the appropriate multiple of $G = 2\pi/a$. This procedure is called "*Reduction to the first Brillouin zone*".

In three dimensions, the $E(\boldsymbol{k})$ bands are already more complicated, even in the case of a vanishing potential, since in (7.16) one now has $\boldsymbol{G}$ contributions in all three coordinate directions. Figure 7.3 shows the $E(\boldsymbol{k})$ curves along k_x in the first Brillouin zone for a simple cubic lattice with vanishing potential.

The effect of a finite but very small potential can now be discussed with reference to Figs. 7.2 and 7.3.

In the one-dimensional problem of Fig. 7.2 there is a degeneracy of the energy values at the edges of the first Brillouin zone, i.e., at $+G/2 = \pi/a$

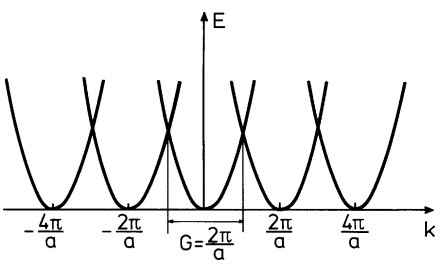

Fig. 7.2. The parabolic energy curves of a free electron in one dimension, periodically continued in reciprocal space. The periodicity in real space is a. This $\boldsymbol{E}(\boldsymbol{k})$ dependence corresponds to a periodic lattice with a vanishing potential ("empty" lattice)

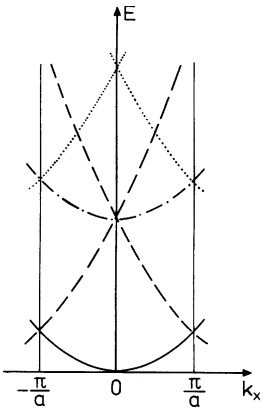

Fig. 7.3. Bandstructure for a free electron gas in a primitive cubic lattice (lattice constant a), represented on a section along k_x in the first Brillouin zone. The periodic potential is assumed to be vanishing ("empty" lattice). The various branches stem from parabolas whose origin in reciprocal space is given by the Miller indices hkl. (——) 000; (– – –) 100, $\bar{1}00$; (–·–) 010, $0\bar{1}0$, 001, $00\bar{1}$; (· · ·) 110, 101, $1\bar{1}0$, $10\bar{1}$, $\bar{1}10$, $\bar{1}01$, $\bar{1}\bar{1}0$, $\bar{1}0\bar{1}$

and $-G/2 = -\pi/a$, where two parabolas intersect. The description of the state of an electron with these k-values is necessarily a superposition of at least two corresponding plane waves. For a vanishing potential (zeroth-order approximation) these waves are

$$e^{iGx/2} \quad \text{and} \quad e^{i[(G/2)-G]x} = e^{-iGx/2} . \tag{7.17}$$

Equation (7.8) implies that waves with G-values larger than $2\pi/a$ must also be taken into account. However, on dividing (7.8) by $[(\hbar^2 k^2/2m)–E]$, it follows that C_k is particularly large when $E_{\boldsymbol{k}}$ and $E_{\boldsymbol{k}-\boldsymbol{G}}$ are both approximately equal to $\hbar^2 k^2/2m$, and that the coefficient $C_{\boldsymbol{k}-\boldsymbol{G}}$ then has approximately the same absolute magnitude as $C_{\boldsymbol{k}}$. This is precisely the case for the two plane waves at the zone boundaries (7.17), and thus, to a first approximation, one can neglect contributions from other reciprocal lattice vectors. The appropriate expressions for a perturbation calculation of the influence of a small potential are therefore of the form

$$\psi_+ \sim (e^{iGx/2} + e^{-iGx/2}) \sim \cos \pi \frac{x}{a} , \tag{7.18 a}$$

$$\psi_- \sim (e^{iGx/2} - e^{-iGx/2}) \sim \sin \pi \frac{x}{a} . \tag{7.18 b}$$

These are standing waves possessing zeros at fixed positions in space. As seen in the discussion of diffraction from periodic structures (Chap. 3), these standing waves can be represented as a superposition of an incoming wave and a counter-propagating "Bragg-reflected" wave. The probability densities, corresponding to ψ_+ and ψ_-,

$$\varrho_+ = \psi_+^* \psi_+ \sim \cos^2 \pi \frac{x}{a} , \tag{7.19 a}$$

$$\varrho_- = \psi_-^* \psi_- \sim \sin^2 \pi \frac{x}{a} , \tag{7.19 b}$$

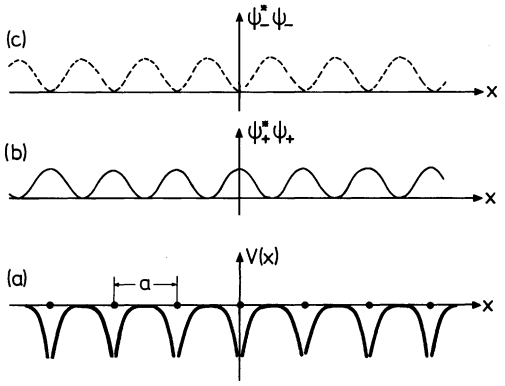

Fig. 7.4. (**a**) Qualitative form of the potential energy $V(x)$ of an electron in a one-dimensional lattice. The positions of the ion cores are indicated by the points with separation a (lattice constant). (**b**) Probability density $\varrho_+ = \psi_+^*\psi_+$ for the standing wave produced by Bragg reflection at $k = \pm\pi/a$ (upper edge of band ① in Fig. 7.5). (**c**) Probability density $\varrho_- = \psi_-^*\psi_-$ for the standing wave at the lower edge of band ② (Fig. 7.5) at $k = \pm\pi/a$

are depicted in Fig. 7.4 together with a qualitative sketch of the potential. For an electron in the state ψ_+, the charge density is maximum at the position of the positive cores and minimum in between; for ψ_- the charge density is maximum between the cores. In comparison with the travelling plane wave e^{ikx}, which is a good approximation to the solution further away from the zone boundary, ψ_+ thus has a lower total energy (particularly potential energy), and ψ_- a higher energy than that of a free electron on the energy parabola (zero potential case). This increase and decrease in the energy of the states at the zone boundary represents a deviation from the free-electron energy parabola (Fig. 7.5).

Having gained insight into the problem from this qualitative discussion, it is now easy to carry out a formal calculation of the magnitude of the so-called band splitting or *energy gap* shown in Fig. 7.5.

Starting from the general representation of the Schrödinger equation in $\boldsymbol{k}$-space (7.8), translation by a reciprocal lattice vector yields

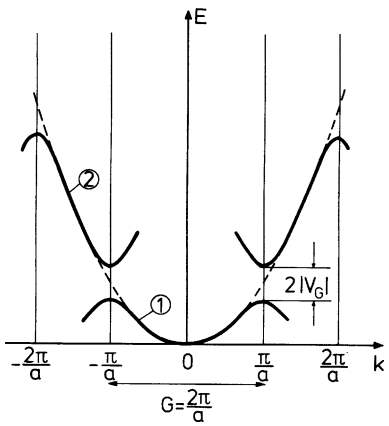

Fig. 7.5. Splitting of the energy parabola of the free electron (– – –) at the edges of the first Brillouin zone $\boldsymbol{k} = \pm\pi/a$ in the one-dimensional case). To a first approximation the gap is given by twice the corresponding Fourier coefficient V_G of the potential. Periodic continuation over the whole of $\boldsymbol{k}$-space gives rise to continuous bands ① and ②, shown here only in the vicinity of the original energy parabola

$$\left(E - \frac{\hbar^2}{2m}|\boldsymbol{k}-\boldsymbol{G}|^2\right) C_{\boldsymbol{k}-\boldsymbol{G}} = \sum_{\boldsymbol{G}'} V_{\boldsymbol{G}'} C_{\boldsymbol{k}-\boldsymbol{G}-\boldsymbol{G}'}$$
$$= \sum_{\boldsymbol{G}'} V_{\boldsymbol{G}'-\boldsymbol{G}} C_{\boldsymbol{k}-\boldsymbol{G}'} \ , \quad \text{i.e.} \tag{7.20 a}$$

$$C_{\boldsymbol{k}-\boldsymbol{G}} = \frac{\sum\limits_{\boldsymbol{G}'} V_{\boldsymbol{G}'-\boldsymbol{G}} C_{\boldsymbol{k}-\boldsymbol{G}'}}{E - \dfrac{\hbar^2}{2m}|\boldsymbol{k}-\boldsymbol{G}|^2} \ . \tag{7.20 b}$$

For small perturbations, a first approximation to the calculation of $C_{\boldsymbol{k}-\boldsymbol{G}}$ can be made by setting the true eigenvalue E that we are seeking equal to the energy of the free electron ($\hbar^2 k^2/2m$). Furthermore, in this first approximation, only the largest coefficients $C_{\boldsymbol{k}-\boldsymbol{G}}$ are of interest; in other words, we expect the greatest deviation from free-electron behavior when the denominator in (7.20 b) vanishes, i.e., for

$$\boldsymbol{k}^2 \simeq |\boldsymbol{k}-\boldsymbol{G}|^2 \ . \tag{7.21}$$

This is identical to the Bragg condition (3.32). The strongest perturbations to the energy surface of the free electron (spheres in $\boldsymbol{k}$-space), produced by the periodic potential, occur when the Bragg condition is satisfied, i.e., for the $\boldsymbol{k}$-vectors at the edge of the first Brillouin zone. It follows from (7.20 b), however, that besides $C_{\boldsymbol{k}-\boldsymbol{G}}$, the coefficient $C_{\boldsymbol{k}}$ is equally important. Thus, in the system of (7.20 a), for this approximation we only need to consider two relations ($V_0 = 0$):

$$\begin{aligned} &\left(E - \frac{\hbar^2}{2m}k^2\right) C_{\boldsymbol{k}} - V_{\boldsymbol{G}} C_{\boldsymbol{k}-\boldsymbol{G}} = 0 \\ &\left(E - \frac{\hbar^2}{2m}|\boldsymbol{k}-\boldsymbol{G}|^2\right) C_{\boldsymbol{k}-\boldsymbol{G}} - V_{-\boldsymbol{G}} C_{\boldsymbol{k}} = 0 \ . \end{aligned} \tag{7.22}$$

We thus obtain the secular equation for the energy value

$$\begin{vmatrix} \left(\dfrac{\hbar^2}{2m}k^2 - E\right) & V_{\boldsymbol{G}} \\ V_{-\boldsymbol{G}} & \left(\dfrac{\hbar^2}{2m}\right)|\boldsymbol{k}-\boldsymbol{G}|^2 - E \end{vmatrix} = 0 \ . \tag{7.23}$$

With $E^0_{\boldsymbol{k}-\boldsymbol{G}} = (\hbar^2/2m)\,|\boldsymbol{k}-\boldsymbol{G}|^2$ as the energy of the free electrons, the two solutions to this secular equation may be written

$$E^{\pm} = \tfrac{1}{2}(E^0_{\boldsymbol{k}-\boldsymbol{G}} + E^0_{\boldsymbol{k}}) \pm \left[\tfrac{1}{4}(E^0_{\boldsymbol{k}-\boldsymbol{G}} - E^0_{\boldsymbol{k}})^2 + |V_{\boldsymbol{G}}|^2\right]^{1/2} \ . \tag{7.24}$$

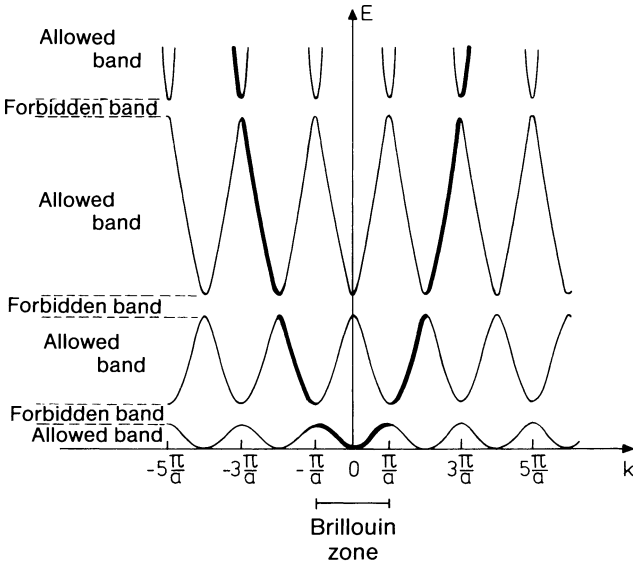

Fig. 7.6. Energy dispersion curves $E(\boldsymbol{k})$ for a one-dimensional lattice (lattice constant a) in the extended zone scheme. As can be seen, the quasi-free-electron approximation gives rise to forbidden and allowed energy regions due to the opening of band gaps, as shown in Fig. 7.5 (cf. the vanishing potential case of Fig. 7.2). The parts of the bands corresponding to the free-electron parabola are indicated by the thick lines

Therefore, at the zone boundary itself, where the contributions of the two waves with $C_{\boldsymbol{k}}$ and $C_{\boldsymbol{k}-\boldsymbol{G}}$ are equal – see (7.21) – and where $E^0_{\boldsymbol{k}-\boldsymbol{G}} = E^0_{\boldsymbol{k}}$, the energy gap has a value

$$\Delta E = E_+ - E_- = 2|V_{\boldsymbol{G}}| \,, \tag{7.25}$$

i.e., twice the $\boldsymbol{G}$th Fourier component of the potential.

Near to the zone boundary, the form of the two energy surfaces that are separated by this gap is described by (7.24) (in which one again sets $E^0_{\boldsymbol{k}} = \hbar^2 k^2/2m$). Figure 7.5 illustrates this for the one-dimensional case near to the zero boundary at $k = G/2$.

The correspondence between the energy parabola of the free electrons and the periodic bandstructure, with its energy gaps due to the realistic potential, is depicted in Figs. 7.5 and 7.6, in both cases for the one-dimensional problem.

7.3 The Tight-Binding Approximation

The electrons that occupy the energetically low-lying core levels of a free atom are strongly localized in space. They naturally retain this strong localization when the atom participates in the formation of a crystal. It thus appears that the description of a solid's electronic structure in terms of

quasi-free electrons must be inadequate. Since these core electrons largely retain the properties that they had in the free atom, an obvious approach is to describe the crystal electrons in terms of a linear superposition of atomic eigenfunctions. This procedure, also known as the LCAO method (Linear Combination of Atomic Orbitals), was already discussed qualitatively in Chap. 1 in relation to chemical bonding, in order to explain the existence of electronic bands in solids.

In formulating the problem, one assumes that the solutions to the Schrödinger equation for the free atoms that form the crystal

$$\mathscr{H}_A(\boldsymbol{r}-\boldsymbol{r_n})\varphi_i(\boldsymbol{r}-\boldsymbol{r_n}) = E_i\varphi_i(\boldsymbol{r}-\boldsymbol{r_n}) \tag{7.26}$$

are known. $\mathscr{H}_A(\boldsymbol{r}-\boldsymbol{r_n})$ is the Hamiltonian for a free atom at the lattice position $\boldsymbol{r_n} = n_1\boldsymbol{a}_1 + n_2\boldsymbol{a}_2 + n_3\boldsymbol{a}_3$ and $\varphi_i(\boldsymbol{r}-\boldsymbol{r_n})$ is the wavefunction for an electron in the atomic energy level E_i. One imagines the entire crystal to be built up of single atoms, i.e., the Hamiltonian for an electron (one-electron approximation!) in the total potential of all the atoms can be written:

$$\mathscr{H} = \mathscr{H}_A + v = -\frac{\hbar^2}{2m}\Delta + V_A(\boldsymbol{r}-\boldsymbol{r_n}) + v(\boldsymbol{r}-\boldsymbol{r_n}) \; . \tag{7.27}$$

The influence of atoms in the neighborhood of $\boldsymbol{r_n}$, where the electron of interest is relatively strongly localized, is described by a perturbation $v(\boldsymbol{r}-\boldsymbol{r_n})$ to the potential V_A of the free atom. This perturbation can thus be expressed as

$$v(\boldsymbol{r}-\boldsymbol{r_n}) = \sum_{\boldsymbol{m}\neq\boldsymbol{n}} V_A(\boldsymbol{r}-\boldsymbol{r_m}) \tag{7.28}$$

i.e., as a sum over the potentials of all atoms apart from that at $\boldsymbol{r_n}$, at the position $\boldsymbol{r}$ of the electron (Fig. 7.7).

We now seek solutions of the Schrödinger equation

$$\mathscr{H}\psi_{\boldsymbol{k}}(\boldsymbol{r}) = E(\boldsymbol{k})\psi_{\boldsymbol{k}}(r) \; , \tag{7.29}$$

where $\mathscr{H}$ is the Hamiltonian of (7.27) for the crystal electron and $\psi_k(\boldsymbol{r})$ are Bloch waves with the general properties discussed in Sect. 7.1.

Multiplying (7.29) by $\psi_{\boldsymbol{k}}^*$ and integrating over the range in which $\psi_{\boldsymbol{k}}$ is defined, one readily obtains

$$E(\boldsymbol{k}) = \frac{\langle\psi_{\boldsymbol{k}}|\mathscr{H}|\psi_{\boldsymbol{k}}\rangle}{\langle\psi_{\boldsymbol{k}}|\psi_{\boldsymbol{k}}\rangle} \; , \tag{7.30}$$

where $\langle\psi_{\boldsymbol{k}}|\psi_{\boldsymbol{k}}\rangle = \int d\boldsymbol{r}\,\psi_{\boldsymbol{k}}^*\psi_{\boldsymbol{k}}$ and $\langle\psi_{\boldsymbol{k}}|\mathscr{H}|\psi_{\boldsymbol{k}}\rangle = \int d\boldsymbol{r}\,\psi_{\boldsymbol{k}}^*\mathscr{H}\psi_{\boldsymbol{k}}$ (cf. Sect. 1.2 and Problem 1.8). If, instead of the true wavefunction, one inserts a trial wavefunction $\Phi_{\boldsymbol{k}}$ into (7.30), then one obtains an energy E' that is always larger than $E(\boldsymbol{k})$. The better $\Phi_{\boldsymbol{k}}$ approximates the true wavefunction, the closer $E'(\boldsymbol{k})$ lies to $E(\boldsymbol{k})$. This circumstance provides the basis for the Ritz procedure.

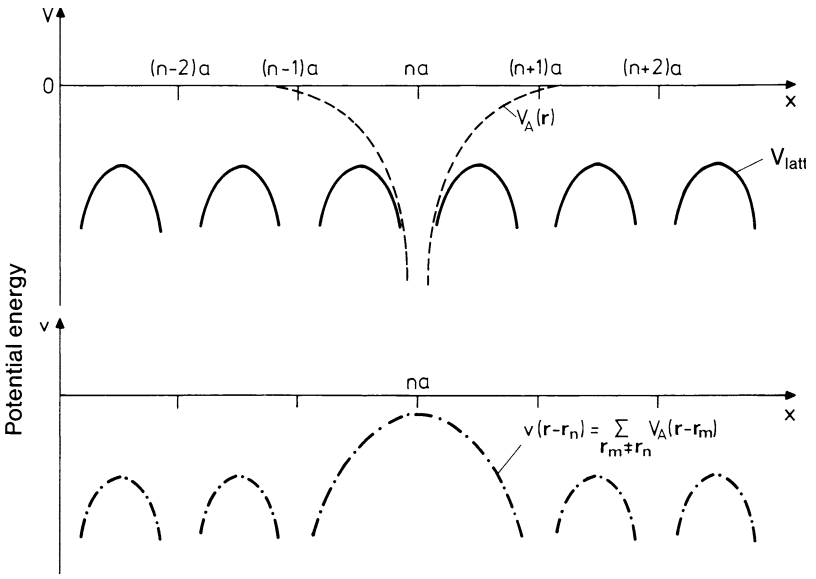

Fig. 7.7. Cross section of the potential used in the tight-binding approximation along the x-direction. The lattice potential V_{latt} (——) is obtained by summing the potentials V_A of the free atoms (– – –). The perturbation potential $v(\boldsymbol{r}-\boldsymbol{r_n})$ used in the approximate calculation is given by the dash-dotted line in the lower part of the figure

In the present case, when we want to calculate the crystal electron energy states $E(\boldsymbol{k})$ that derive from the energy level E_i of the free atom, we assume that a good approximation to $\psi_{\boldsymbol{k}}$ is provided by a linear combination of atomic eigenfunctions $\varphi_i(\boldsymbol{r}-\boldsymbol{r_n})$, i.e.,

$$\psi_{\boldsymbol{k}} \approx \Phi_{\boldsymbol{k}} = \sum_{\boldsymbol{n}} a_{\boldsymbol{n}} \varphi_i(\boldsymbol{r}-\boldsymbol{r_n}) = \sum_{\boldsymbol{n}} \mathrm{e}^{\mathrm{i}\boldsymbol{k}\cdot\boldsymbol{r_n}} \varphi_i(\boldsymbol{r}-\boldsymbol{r_n}) \; . \tag{7.31}$$

The expansion coefficients are determined as $a_{\boldsymbol{n}} = \exp(\mathrm{i}\boldsymbol{k}\cdot\boldsymbol{r_n})$ by the requirement that Φ_k should be a Bloch wave. It can easily be shown that $\Phi_{\boldsymbol{k}}$ in (7.31) possesses all the required properties of Bloch waves (Sect. 7.1), e.g.,

$$\Phi_{\boldsymbol{k}+\boldsymbol{G}} = \sum_{\boldsymbol{n}} \mathrm{e}^{\mathrm{i}\boldsymbol{k}\cdot\boldsymbol{r_n}} \mathrm{e}^{\mathrm{i}\boldsymbol{G}\cdot\boldsymbol{r_n}} \varphi_i(\boldsymbol{r}-\boldsymbol{r_n}) = \Phi_{\boldsymbol{k}} \; . \tag{7.32}$$

An approximate calculation of $E(\boldsymbol{k})$ can now be made by inserting in (7.30) the trial function of (7.31); the denominator in (7.30) becomes:

$$\langle \Phi_{\boldsymbol{k}} | \Phi_{\boldsymbol{k}} \rangle = \sum_{\boldsymbol{n},\boldsymbol{m}} \mathrm{e}^{\mathrm{i}\boldsymbol{k}\cdot(\boldsymbol{r_n}-\boldsymbol{r_m})} \int \varphi_i^*(\boldsymbol{r}-\boldsymbol{r_m}) \varphi_i(\boldsymbol{r}-\boldsymbol{r_n}) d\boldsymbol{r} \; . \tag{7.33}$$

For a sufficiently localized electron, $\varphi_{\boldsymbol{k}}(\boldsymbol{r}-\boldsymbol{r_m})$ only has significant values in the vicinity of $\boldsymbol{r_m}$. Thus, to a first approximation, we only retain terms in (7.33) with $\boldsymbol{n} = \boldsymbol{m}$, and obtain

$$\langle \Phi_{\boldsymbol{k}} | \Phi_{\boldsymbol{k}} \rangle \simeq \sum_{\boldsymbol{n}} \int \varphi_i^*(\boldsymbol{r} - \boldsymbol{r}_{\boldsymbol{n}}) \varphi_i(\boldsymbol{r} - \boldsymbol{r}_{\boldsymbol{n}}) d\boldsymbol{r} = N \,, \tag{7.34}$$

where N is the number of atoms in the crystal.

Making use of the fact we know the solutions to (7.26) for the free atom, we write

$$E(\boldsymbol{k}) \approx \frac{1}{N} \sum_{\boldsymbol{n},\boldsymbol{m}} \mathrm{e}^{\mathrm{i}\,\boldsymbol{k}\cdot(\boldsymbol{r}_{\boldsymbol{n}} - \boldsymbol{r}_{\boldsymbol{m}})} \int \varphi_i^*(\boldsymbol{r} - \boldsymbol{r}_{\boldsymbol{m}}) [E_i + v(\boldsymbol{r} - \boldsymbol{r}_{\boldsymbol{n}})] \varphi_i(\boldsymbol{r} - \boldsymbol{r}_{\boldsymbol{n}}) d\boldsymbol{r} \tag{7.35}$$

where E_i is the energy eigenvalue of the isolated atom. In the term containing E_i we have again neglected the overlap between nearest neighbors (i.e., only terms with $\boldsymbol{n} = \boldsymbol{m}$ are considered). For the term containing the perturbation $v(\boldsymbol{r} - \boldsymbol{r}_{\boldsymbol{n}})$, overlap is included only up to nearest neighbors. In the simple case when the relevant atomic state φ_i possesses spherical symmetry, i.e., s-character, the result can be readily represented with the help of the following two quantities:

$$A = -\int \varphi_i^*(\boldsymbol{r} - \boldsymbol{r}_{\boldsymbol{n}}) v(\boldsymbol{r} - \boldsymbol{r}_{\boldsymbol{n}}) \varphi_i(\boldsymbol{r} - \boldsymbol{r}_{\boldsymbol{n}}) d\boldsymbol{r} \,, \tag{7.36 a}$$

$$B = -\int \varphi_i^*(\boldsymbol{r} - \boldsymbol{r}_{\boldsymbol{m}}) v(\boldsymbol{r} - \boldsymbol{r}_{\boldsymbol{n}}) \varphi_i(\boldsymbol{r} - \boldsymbol{r}_{\boldsymbol{n}}) d\boldsymbol{r} \tag{7.36 b}$$

and reads

$$E(\boldsymbol{k}) \approx E_i - A - B \sum_{\boldsymbol{m}} \mathrm{e}^{\mathrm{i}\,\boldsymbol{k}\cdot(\boldsymbol{r}_{\boldsymbol{n}} - \boldsymbol{r}_{\boldsymbol{m}})} \,. \tag{7.37}$$

The sum over $\boldsymbol{m}$ includes only values for which $\boldsymbol{r}_{\boldsymbol{m}}$ denotes a nearest neighbor of $\boldsymbol{r}_{\boldsymbol{n}}$.

In the present case, A is positive since v is negative. Equation (7.37), applied to the case of a primitive cubic lattice with

$$\boldsymbol{r}_{\boldsymbol{n}} - \boldsymbol{r}_{\boldsymbol{m}} = (\pm a, 0, 0)\,; \quad (0, \pm a, 0)\,; \quad (0, 0, \pm a) \,,$$

gives, for an atomic s-state,

$$E(\boldsymbol{k}) \approx E_i - A - 2B(\cos k_x a + \cos k_y a + \cos k_z a) \,. \tag{7.38}$$

When the atoms are brought together to form a crystal (with primitive cubic lattice), the atomic energy level E_i therefore becomes an electronic band whose center of gravity is reduced by an amount A with respect to E_i and whose width is proportional to B. This situation is illustrated in Fig. 7.8.

The important consequences can be summarized as follows:

i) Since the cosine terms vary between $+1$ and -1, the width of the energy band is $12\,B_i$. For small $\boldsymbol{k}$-values, the cosine terms can be expanded such that near to the Γ-point (center of the first Brillouin zone at $\boldsymbol{k} = 0$) one obtains

$$E(\boldsymbol{k}) = E_i - A - 6B + B\,a^2 k^2 \,, \tag{7.39}$$

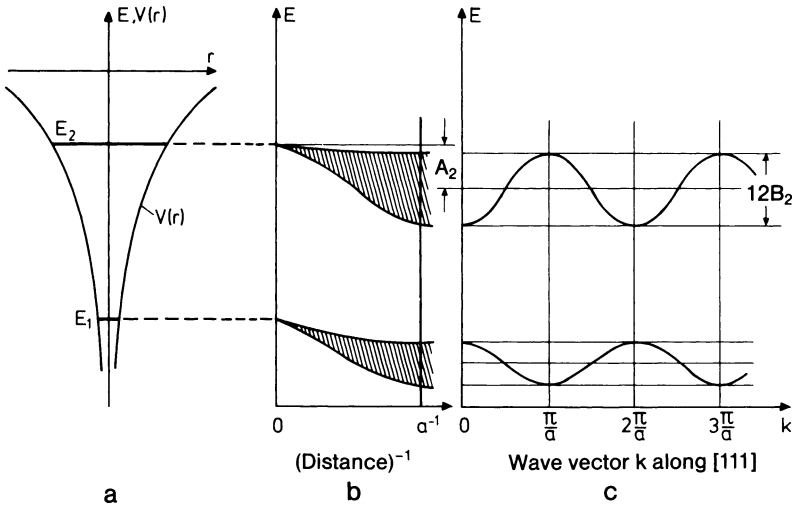

Fig. 7.8 a–c. Qualitative illustration of the result of a tight-binding calculation for a primitive cubic lattice with lattice constant a. (**a**) Position of the energy levels E_1 and E_2 in the potential $V(\boldsymbol{r})$ of the free atom. (**b**) Reduction and broadening of the levels E_1 and E_2 as a function of the reciprocal atomic separation r^{-1}. At the equilibrium separation a the mean energy decrease is A and the width of the band is $12B$. (**c**) Dependence of the one-electron energy E on the wave vector $k(1,1,1)$ in the direction of the main diagonal [111]

where $k^2 = k_x^2 + k_y^2 + k_z^2$. This k^2-dependence corresponds to that which results from the quasi-free-electron approximation (Sect. 7.2).

ii) From (7.36b) it follows that the energy width of the band becomes greater as the overlap between the corresponding wavefunctions of neighboring atoms increases. Lower lying bands that stem from more strongly localized states are thus narrower than bands originating from less strongly bound atomic states whose wavefunctions are more extended.

iii) In the framework of the present one-electron approximation, the occupation of the one-electron band states is obtained by placing two of the available electrons of every atom into each band, beginning with the lowest energy band, until all electrons have been accommodated. The Pauli principle allows the double occupation because of the two possible spin states of the electron.

If a crystal with a primitive cubic lattice contains N atoms, and thus N primitive unit cells, then an atomic energy level E_i of the free atom will split, due to the interaction with the other (N–1) atoms, into N states. These then form the corresponding quasi-continuous band. This band can thus be occupied by $2N$ electrons. We obtain the same result by considering this problem in terms of the quasi-free-electron model: In $\boldsymbol{k}$-space each electron state corresponds to a volume $(2\pi)^3/V$ (where V is the macroscopic crystal volume). The volume of the first Brillouin zone, however, is $(2\pi)^3/V_c$

(where V_c is the volume of the unit cell). Thus the part of the band within the first Brillouin zone contains $V/V_c = N$ states, which, when the two spin states are considered, yields $2N$ states available for occupation by electrons.

The existence of a bandstructure arising from the discrete energy levels of isolated atoms upon their joining together to form a crystal was illustrated qualitatively in Fig. 1.1. For sodium, for example, the atomic $3s$- and $3p$-levels give rise, in the crystal (equilibrium atomic separation r_0), to bands that overlap. Since the occupied levels of atomic sodium are $1s^2, 2s^2, 2p^6, 3s^1$, the atomic $3s$-level only contributes one electron per unit cell to the $3s$-band of the crystal, which could, however, accommodate two electrons per unit cell. Thus, even without the $3s$-$3p$ overlap (analogous to the $2s$–$2p$ overlap in Fig. 1.1), the $3s$ band of Na would only be half full. In Sect. 9.2 we will see that this partial occupation of a band is the source of the metallic conductivity of Na. Qualitative arguments concerning the conductivity have already been presented in Sect. 1.4.

It is well known that isolated carbon atoms have the electronic configuration $1s^2, 2s^2, 2p^2$. However, in the diamond crystal, as a result of the forma-

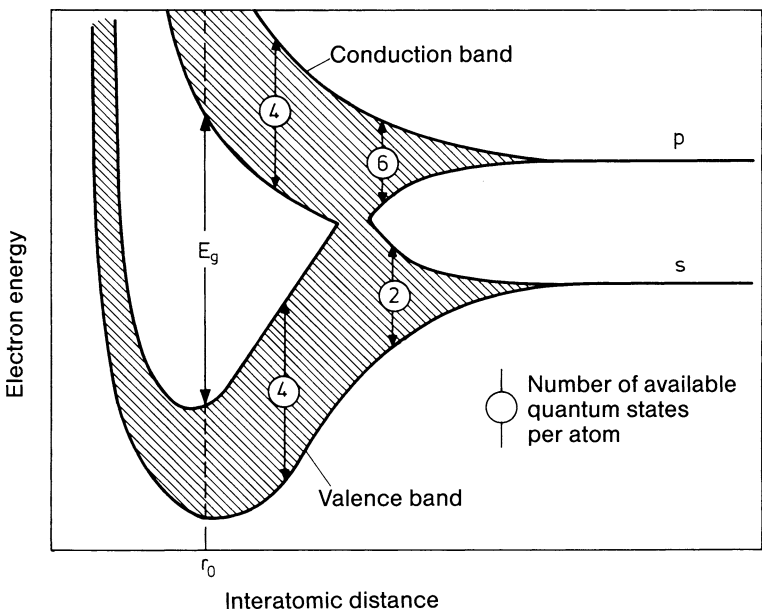

Fig. 7.9. Schematic behavior of the energy bands as a function of atomic separation for the tetrahedrally bound semiconductors diamond (C), Si, and Ge. At the equilibrium separation r_0 there is a forbidden energy gap of width E_g between the occupied and unoccupied bands that result from the sp^3 hybrid orbitals. For diamond, the sp^3 hybrid stems from the $2s$ and $2p^3$ atomic states, for Si from the $3s$ and $3p^3$, and for Ge from the $4s$ and $4p^3$. One sees from this figure that the existence of a forbidden energy region is not tied to the periodicity of the lattice. Thus amorphous materials can also display a band gap. (After [7.1])

tion of the sp^3 hybrid (a mixture of $2s$ and $2p$ wavefunctions with tetrahedral bonding; Chap. 1), there is a modification of the s- and p-levels which manifests itself in a further splitting of the sp^3 hybrid band into two bands, each of which (including spin) can accommodate four electrons (Fig. 7.9).

The four electrons of the atomic $2s$- and $2p$-states thus fill the lower part of the sp^3 band, leaving the upper part unoccupied. Between the two sp^3 subbands there is a forbidden energy gap of width E_g. This is the origin of the insulating property of diamond, as will be shown in Sects. 9.2 and 12.1. The semiconductors Si and Ge are similar cases (Chap. 12).

The form of the bandstructure shown in Fig. 7.9 cannot be derived using the simple approach outlined here. More complex methods are necessary for this calculation and these require the use of modern computing facilities. For further information about such calculations the reader is referred to theoretical reviews and more advanced text books.

7.4 Examples of Bandstructures

In the preceding sections, the origin of the electronic bandstructure, i.e., the existence of allowed and forbidden energy regions for a crystal electron, was attributed to the presence of Bragg reflections, which cause certain regions of the continuous spectrum of free-electron states to become forbidden. The alternative, but equally important, approach starts from the discrete energy levels of the free atom and explains the evolution of bands as a quasi-continuous splitting of the atomic levels due to the interaction with the other atoms of the crystal. In this picture, each band corresponds to an energy level of the free atom and may thus be classified as an s-, p-, or d-band etc. Having given a qualitative picture of a typical metal and a typical insulator in the examples of Figs. 1.1 and 7.9, in this section we will examine a few further examples of realistic bandstructures. Figure 7.10 shows how the highest occupied bands of the ionic crystal KCl can be imagined to evolve from the energy levels of isolated K^+ and Cl^- ions as they approach one another until they reach the equilibrium separation in the crystal. Even at this equilibrium separation, which is known from X-ray diffraction data, the occupied bands are extremely narrow. This indicates that there is relatively little overlap between the charge clouds of the individual ions. If theoretical results such as those shown in Fig. 7.10 are in good agreement with experimental data, then they allow important conclusions to be drawn about the form of the chemical bonding.

The entire information about the one-electron states in the periodic potential is of course contained in a representation of the complete $E(\boldsymbol{k})$ surfaces in wave-vector space. In order to simply portray the often complicated surfaces, one considers cross sections through the energy surfaces along directions of high symmetry in the first Brillouin zone. This is illustrated in Fig. 7.11a for the example of an Al crystal. The definitions of the

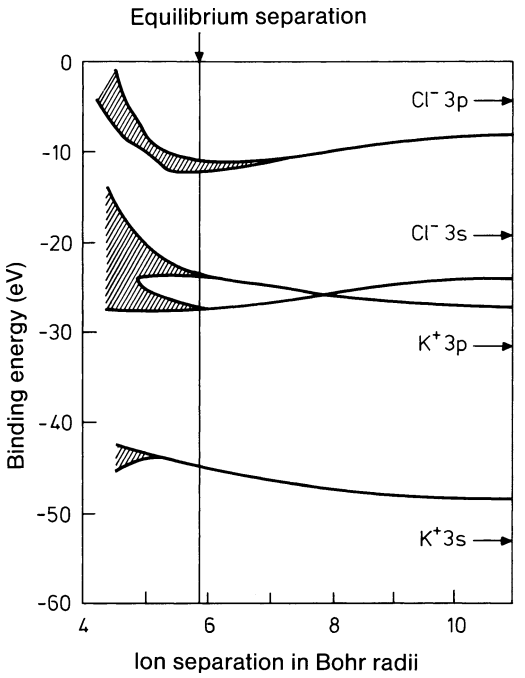

Fig. 7.10. The four highest occupied energy bands of KCl calculated as a function of the ionic separation in Bohr radii ($a_0 = 5.29 \times 10^{-9}$ cm). The energy levels in the free ions are indicated by arrows. (After [7.2])

symmetry directions and symmetry points in the first Brillouin zone of a face-centered cubic lattice are indicated in Figs. 3.8 and 7.11 b.

A striking feature of the Al bandstructure is that it can be described very well by the parabolic dependence of a free-electron gas (dotted lines). The energy gaps at the Brillouin zone edges are relatively small and the

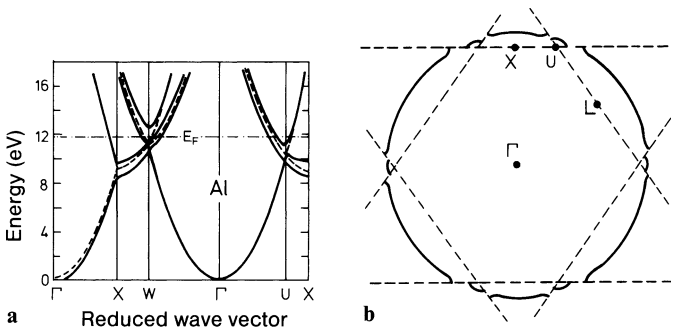

Fig. 7.11. (**a**) Theoretical bandstructure $E(\boldsymbol{k})$ for Al along directions of high symmetry (Γ is the center of the Brillouin zone). The dotted lines are the energy bands that one would obtain if the *s*- and *p*-electrons in Al were completely free ("empty" lattice). After [7.3]. (**b**) Cross section through the Brillouin zone of Al. The zone edges are indicated by the dashed lines. The Fermi "sphere" of Al (——) extends beyond the edges of the first Brillouin zone

complexity of the bandstructure stems largely from the fact that the energy parabolas are plotted in the reduced-zone scheme, i.e.,"folded" back into the first Brillouin zone. This type of bandstructure is characteristic for simple metals. The similarity to the free electron gas is particularly pronounced for the alkali metals Li, Na and K.

The filling of the bands with the available electrons continues up to the Fermi energy E_F (indicated in Fig. 7.11). It can be seen that the corresponding constant energy surface, the so-called Fermi surface $E(\boldsymbol{k}) = E_F$, intersects several bands. Thus, even for Al, the Fermi surface is not a simple continuous surface: whereas the Fermi surfaces of the alkali metals are almost spherical and are contained wholly within the first Brillouin zone, the "Fermi sphere" of Al extends just beyond the edges of the first Brillouin zone. The Bragg reflections occurring at these edges cause a slight deviation from the spherical form in these regions. This is shown qualitatively in Fig. 7.11 b in a cross section through three-dimensional $\boldsymbol{k}$-space.

In comparison to the simple metals, the band structures of the transition metals are considerably more complicated, due to the significant influence

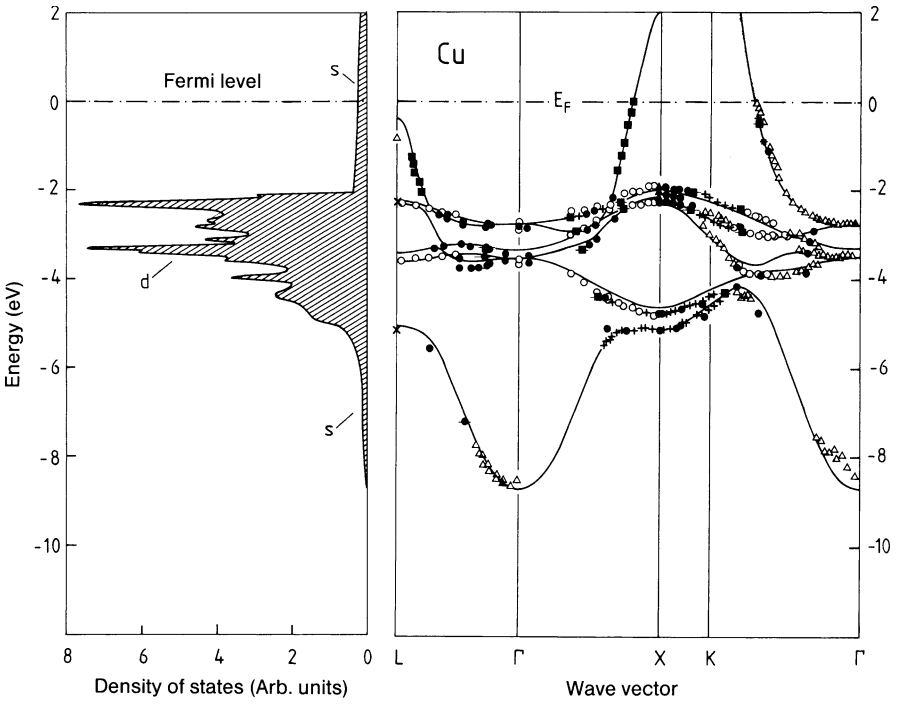

Fig. 7.12. Bandstructure $E(\boldsymbol{k})$ for copper along directions of high crystal symmetry (*right*). The experimental data were measured by various authors and were presented collectively by Courths and Hüfner [7.4]. The full lines showing the calculated energy bands and the density of states (*left*) are from [7.5]. The experimental data agree very well, not only among themselves, but also with the calculation

of the *d*-bands. Together with the bands that originate from *s*-levels and resemble the parabolic form of the free-electron gas, there are also very flat $E(\boldsymbol{k})$ bands, whose small energy width (low dispersion) can be attributed to the strong localization of the *d*-electrons. This is readily seen for the example of copper, whose bandstructure is illustrated in Fig. 7.12. For transition metals such as Pt, W, etc., where the Fermi level intersects the complex *d*-bands, the Fermi surfaces possess particularly complicated forms.

Other interesting phenomena, such as semiconducting properties (Chap. 12), occur when the bandstructure possesses an absolute gap, i.e., a so-called forbidden region: in this particular energy range and for all $\boldsymbol{k}$-directions in reciprocal space, there are no available electron states. A typical bandstructure of this type is that of germanium (Fig. 7.13). Like diamond and silicon, germanium crystallizes in the diamond structure, whereby the tetrahedral bonding of the individual atoms is a consequence of the formation of sp^3 hybrid orbitals. As was mentioned at the end of Sect. 7.3, the formation of sp^3 hybrids leads to the existence of sp^3 sub-

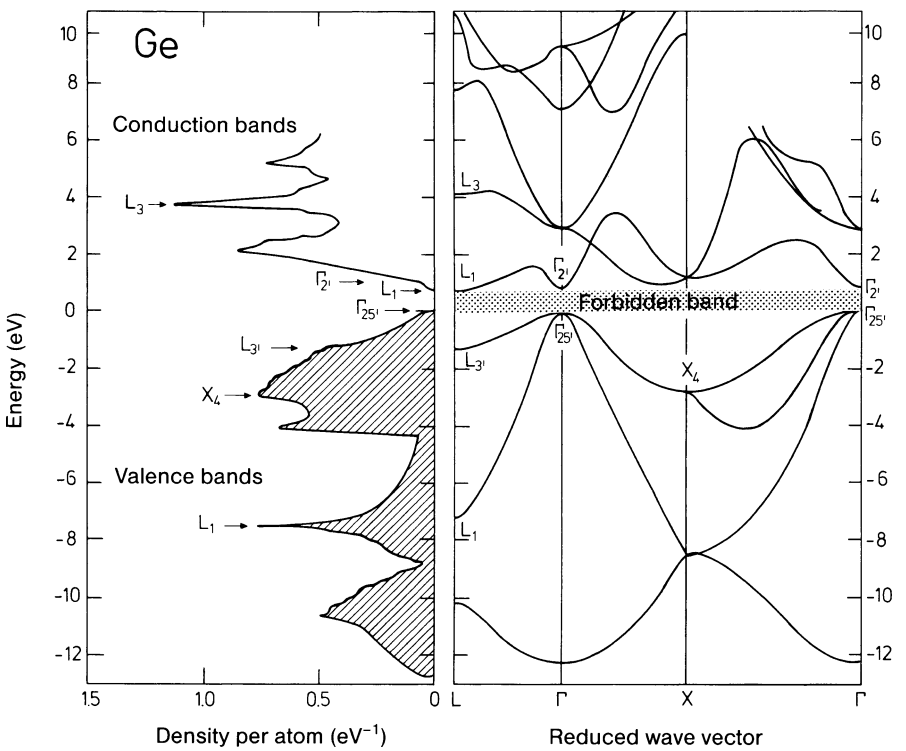

Fig. 7.13. Theoretically derived bandstructure $E(\boldsymbol{k})$ for germanium along directions of high symmetry (*right*), and the corresponding electronic density of states (*left*). A number of critical points, denoted according to their position in the Brillouin zone (Γ, X, L), can be seen to be associated with regions of the bandstructure where $E(\boldsymbol{k})$ has a horizontal tangent. The shaded region of the density of states corresponds to the states occupied by electrons [7.6]

bands. The lower of these (below the forbidden gap) are fully occupied whereas the higher-lying sp^3 subbands above the gap are unoccupied. The Fermi energy must therefore lie within the forbidden gap, a fact that will be important when we come to discuss the semiconducting properties of this crystal in Chap. 12.

7.5 The Density of States

In analogy to the thermal properties of the phonon system (Chap. 5), one finds also in the case of electronic states, that a knowledge of the density of states is sufficient to describe e.g. the energy content of the electron system. For certain electronic excitation mechanisms (e.g. non-angle-resolved photoemission spectroscopy; Panel V), in which the experiment effectively integrates over all $\boldsymbol{k}$-directions, one can often interpret the spectra simply in terms of the number of electron states per energy interval dE.

Once the energy surfaces $E(\boldsymbol{k})$ of the bandstructure are known, then in analogy to (5.4), the density of states is obtained by integrating over an energy shell $\{E(\boldsymbol{k}), E(\boldsymbol{k}) + dE\}$ in $\boldsymbol{k}$-space:

$$dZ = \frac{V}{(2\pi)^3} \int_E^{E+dE} d\boldsymbol{k} \,, \tag{7.40}$$

where $V/(2\pi)^3$ is the density of states in $\boldsymbol{k}$-space. If the volume element $d\boldsymbol{k}$ is separated into an area element df_E on the energy surface and a component $dk_\perp$ normal to this surface (Fig. 5.1), i.e., $d\boldsymbol{k} = df_E dk_\perp$, then with $dE = |\mathrm{grad}_{\boldsymbol{k}} E|\, dk_\perp$ one has

$$D(E)dE = \frac{1}{(2\pi)^3} \left(\int_{E(\boldsymbol{k})=\mathrm{const}} \frac{df_\mathrm{E}}{|\mathrm{grad}_{\boldsymbol{k}} E(\boldsymbol{k})|} \right) dE \,. \tag{7.41}$$

This density of states $D(E)$ is given here in relation to the real volume V of the crystal in order to obtain a crystal-specific quantity. It should be remembered that, due to spin degeneracy, each state can accommodate two electrons.

The main structure in the function $D(E)$ is again yielded by those points in $\boldsymbol{k}$-space for which $|\mathrm{grad}_{\boldsymbol{k}} E|$ vanishes, i.e., where the energy surfaces are flat. These points are known as van Hove singularities or critical points. In three dimensions $D(E)$ does not become singular near to these critical points because an expansion of $E(\boldsymbol{k})$ about the extremum ($E \sim \boldsymbol{k}^2$) implies that $|\mathrm{grad}_{\boldsymbol{k}} E|^{-1}$ has a k^{-1} singularity. Thus the integration of the $E(\boldsymbol{k})$ surface (7.41) yields a linear k dependence. In three dimensions the density of states near to a critical point therefore has the form shown in Fig. 7.14. For one-dimensional bandstructures, which, to a good approximation, can be used

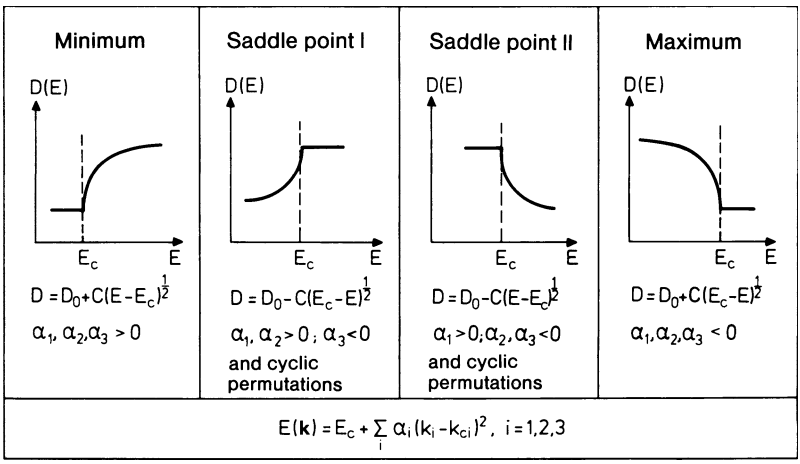

Fig. 7.14. Form of the density of states $D(E)$ in the vicinity of the four possible types of critical point in three dimensions. The energy of the critical points is denoted by E_c and the corresponding $\boldsymbol{k}$-space position by k_{ci} $(i = 1,2,3)$. In the parabolic approximation, the energy band has the form $E(\boldsymbol{k}) = E_c + \sum_i \alpha_i \cdot (k_i - k_{ci})^2$ in the vicinity of a critical point, where $\alpha_i = \text{const}$. The quantities D_0 and C in the figure are also constants

to describe one-dimensional organic semiconductors, the density of states diverges at the critical points, although its integral remains finite. (See discussion of density of states of lattice vibrations for a linear chain; Sect. 4.3.)

Theoretical densities of states may be obtained by integrating in $\boldsymbol{k}$-space over the first Brillouin zone for a calculated bandstructure, and may then be compared with experimental data, for example from photoemission spectroscopy (Panel V). As such, they provide an important point of connection between calculated bandstructures and the experimental data. In the integration over $\boldsymbol{k}$-space the main contributions to the density of states are derived from the critical points. Since the critical points usually occur along lines of, or at points of high symmetry in $\boldsymbol{k}$-space, this lends further justification for the preferred representation of bandstructures along lines of high symmetry, e.g., $\Gamma K, \Gamma X, \Gamma L$, etc. In the intermediate regions one can expect only minor contributions, and it is sometimes possible to make use of simple mathematical interpolation to obtain the bandstructure there.

The relationship between a calculated bandstructure and the corresponding density of states is nicely demonstrated by the case of the semiconductor germanium as shown in Fig. 7.13. Important contributions, i.e., maxima in the density of states, are clearly correlated with flat portions of the $E(\boldsymbol{k})$ curves along directions of high symmetry. Also evident is the absolute band gap between the fully occupied valence band states and the (at low temperatures) unoccupied conduction band states. This forbidden region has a width of about 0.7 eV for germanium.

As an example for a transition metal, Fig. 7.12 shows the calculated density of states for copper. The density of states is obtained by integrating

over the bandstructure $E(\boldsymbol{k})$, which is also shown in the figure. The sharp structures seen between –2 and –6 eV below the Fermi level can be readily attributed to critical points of the relatively flat *d*-bands. In the $E(\boldsymbol{k})$ plot (Fig. 7.12) one can also recognize the parabola-like shape of the *s*-band with its minimum at the Γ-point. This *s*-band is responsible for the structureless contribution to the density of states beginning at about –9.5 eV. Below –6 eV one cannot fail to notice the distinct similarity to the "free-electron-gas" parabolic density of states. At the Fermi level it is again the *s*-electrons that produce the density of states. This explains why the model of a free-electron gas in a box (Chap. 6) yields relatively good results for copper.

However, as shown in Sect. 6.4, this is far from true for Fe, Ni, Co and the other transition metals. For these metals the Fermi level intersects the high density of states of the *d*-bands, which are therefore only partially filled. For the ferromagnets Fe, Ni and Co there is an additional complication, which will be dealt with in detail in Sect. 8.3. In these metals there is a ferromagnetic phase at $T < T_C$ (Curie Temperature) in which the atomic spins are aligned. One then has two distinct densities of states – one for electrons whose spin is parallel to the spontaneous magnetization $\boldsymbol{M}$ and one for the electrons with antiparallel spin orientation. Figure 8.6 shows these two densities of states for Ni. To derive such densities of states requires a calculated bandstructure $E(\boldsymbol{k})$ in which the electron–electron interaction is explicitly included.

7.6 Density of States in Non-Crystalline Solids

A crystalline solid is translationally invariant with respect to a lattice vector and the electronic states can be classified according to the components of the wave-vector k_x, k_y, and k_z. Only then are the eigen-values of the electronic states described by a band structure $E(\boldsymbol{k})$. However, the concept of a density of states per energy and volume and of allowed and forbidden bands does not require translational invariance. Thus, a non-crystalline solid possesses a defined density of states, just as the crystalline solid, provided that the non-crystalline solid is sufficiently homogeneous in composition and structure on a mesoscopic length scale. Many materials exist in a crystalline as well as non-crystalline phases, as under-cooled melts (glasses). Examples are SiO_2 and Al_2O_3. As is well known, these two materials are optically transparent in either phase. Both phases must therefore have an energy gap between occupied and unoccupied states larger than 3 eV. Thus it seems that the magnitude of the energy gap does not depend on the existence of crystalline order. The amorphous phases of SiO_2 and Al_2O_3, and likewise the amorphous phases of Si and Ge differ from the crystalline phases only by the missing long-range order. The nearest and next nearest neighbor configuration is rather similar. In Si and Ge the local order is

determined by the sp^3-bonding to the nearest-neighbors. Since the electronic structure is dominated by the local bonding, the magnitude of the energy gap is nearly equal for the crystalline and the amorphous phases. Likewise the densities of states for other electron energies are rather similar. Only the sharp features in the band structure resulting from the critical points (Fig. 7.13) are absent in the amorphous phases.

Amorphous phases of Si and Ge can be fabricated by growth at (relatively) low temperatures. At these temperatures long-range order, which requires diffusion of material, is not established and the state of lowest free enthalpy which is the crystalline phase, is not reached. In order to saturate nevertheless as many bonds as possible the sp^3-tetraeders of the local bonding configuration must be slightly distorted. Hence, instead of defined nearest-neighbor bond angles and bond distances the amorphous phase possesses a (narrow Gaussian) distribution of bond angles and distances. As shown in Fig. 7.9 the magnitude of the energy gap depends on the distance between the nearest-neighbors. The fuzzy distribution of bond distances in amorphous solids therefore leads to a fuzzy band gap: the density of states acquires exponential tails that extend into the forbidden zone (Fig. 7.15). The magnitude of the density of states at any energy reflects the probability for the realization of a particular bond distance and bond angle. States that reach far into the forbidden zone (forbidden in crystals) are due to structural configurations that are realized only rarely. The mean distance between such configurations is therefore large and consequently the wave functions of these states do not overlap. Electronic states deeper in the for-

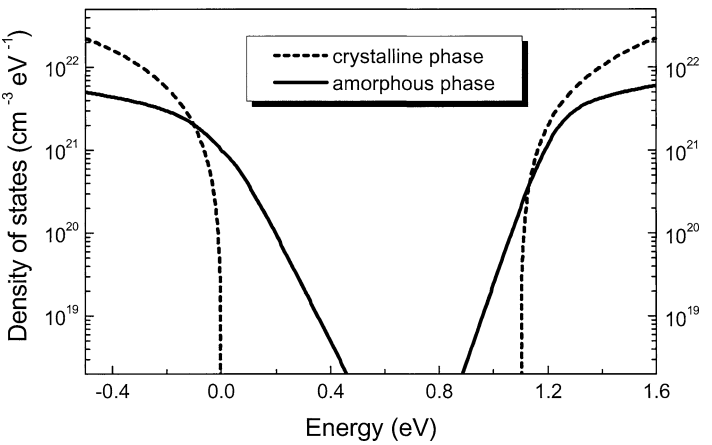

Fig. 7.15. Schematic density of states of an ideal amorphous material with saturated tetrahedral bonds to the nearest-neighbors (*full line*). The numbers for the density of states correspond to amorphous silicon. Compared to crystalline silicon (*dashed line*) the density of states possesses exponential tails into the band gap. Non-saturated bonds in the amorphous network lead to additional states in the forbidden zone. For practical applications of amorphous silicon (e.g. in solar cells) one attempts to reduce the number of unsaturated bonds by adding hydrogen

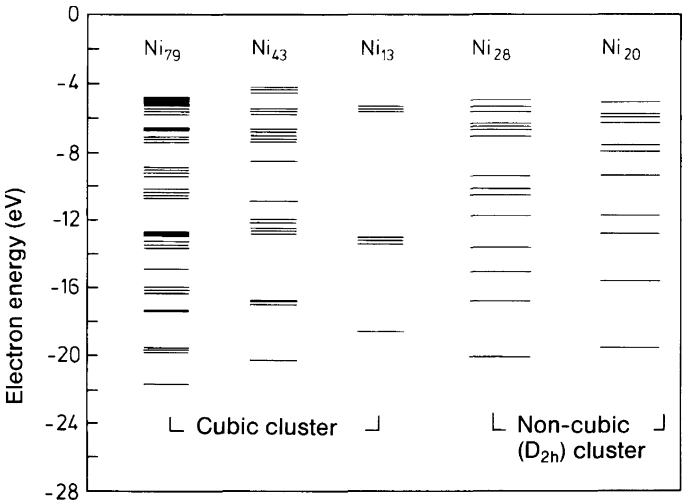

Fig. 7.16. Calculated energy terms below the Fermi level for cubic Ni-clusters consisting of 13, 43, and 79 atoms and non-cubic clusters of the symmetry D_{2h} with 20 and 28 atoms [7.7]. The energy scale refers to the vacuum level. States displayed as thick lines consist of several, nearly degenerate states. The work function of the solid (5.2 eV [6.5]) as well as the high density of *d*-states at the Fermi level is quite well represented by the cluster with 79 atoms

bidden zone are therefore localized in space. Electrons in these states are not free to move about, unlike the electrons in Bloch states (see also Sect. 9.8).

The calculation of electronic states in "amorphous" solids is significantly more difficult than for crystalline solids. This is in part due to the fact that the characterization of a solid as being amorphous is not a well-defined one. While the atom positions in a crystal are unique, an infinite number of different realizations of an amorphous solid exist. A calculation of the electronic density of states of an amorphous solid requires the input of a particular distribution of bond angles and distances. With that input, one may compose a structure of an amorphous solid and treat this agglomeration of atoms as a large molecule. Such molecules consisting of many atoms or atomic units of the same type are named "clusters". The electronic states of clusters are discrete because of the finite number of atoms that make up the cluster. With increasing number of atoms in the cluster a continuous density of states can be defined. Technically, a density of states is frequently calculated by broadening the individual states artificially (Fig. 7.16). Theoretical methods to extend clusters into all three dimensions in a non-periodic way have also been developed.

Initially, clusters were merely a construct of the theorists to calculate the electronic properties of amorphous solids. Since the experimental realization of clusters with a defined size and composition [7.8], research on clusters has become a field of its own, situated between Moleculer Physics, Solid State Physics, and Material Science.

Problems

7.1 Solve the Schrödinger equation for the potential

$$V(x, y, z) = \begin{cases} \infty, & x < 0 \\ 0, & x \geq 0 \end{cases}$$

and calculate the charge density

$$\varrho(x, y, z) = (-2\,\mathrm{e}) \sum_{k_x, k_y, k_z} |\Psi_{\boldsymbol{k}}|^2 \,,$$

where the maximum $\boldsymbol{k}$ value is determined by the Fermi energy E_F. Sketch $\varrho(x)$ and discuss the result (Friedel oscillations). Consider the cases of a typical metallic electron density of $10^{22}\,\mathrm{cm}^{-3}$ and of a weakly doped semiconductor with a density of $10^{16}\,\mathrm{cm}^{-3}$.

7.2 A two-dimensional electron gas is described in reciprocal space by a two-dimensional lattice whose Brillouin zone is a primitive square.

a) Show that the kinetic energy of a free electron in a corner of the first Brillouin zone is a factor of two larger than that of an electron with k vector in the middle of the Brillouin-zone edge.
b) How large is the corresponding factor for a primitive lattice in three dimensions?
c) Show that band overlap can occur even in a two-dimensional lattice. Do this by drawing the following dispersion relations for the case of free electrons that are perturbed by a weak periodic potential:

$$E(k_y) \quad \text{for} \quad k_x = 0 \,,$$
$$E(k_y) \quad \text{for} \quad k_x = \frac{\pi}{a} \,,$$
$$E(k) \quad \text{for} \quad k_x = k_y \,.$$

7.3 As a simple model of a crystal consider a one-dimensional chain of $2N$ atoms at distances a_0 from each other. Let $\phi_i(x–n\,a_0)$ be the correct wavefunction for an electron with energy E_i at the atom located at $n\,a_0$ (eigenvalue for a single-isolated atom). Under what conditions can the one-electron wavefunction $\Psi(x)$ for an electron delocalized over the whole chain of atoms be approximated by a linear combination of atomic orbitals (LCAO)

$$\Psi(x) \cong \sum_{n=-N}^{N} c_n \phi_i(x - n\,a_0) \;?$$

Choose the coefficients c_n such that for $N \to \infty$ the wave-function $\Psi(x)$ is a Bloch wave.

7.4 a) Consider points in the vicinity of the minimum of an electronic band at sufficiently small k values that $E(\boldsymbol{k})$ can be written in parabolic approximation as

$$E(\boldsymbol{k}) = E_c + \frac{\hbar^2}{2}\left(\frac{k_x^2}{m_x} + \frac{k_y^2}{m_y} + \frac{k_z^2}{m_z}\right),$$

with m_x, m_y and m_z as positive constants. Show that the density of states $D(E)$ is proportional to $(E–E_c)^{1/2}$ around the critical point $E_c(\boldsymbol{k} = \boldsymbol{0})$.

b) Consider the density of states in the neighborhood of a saddle point, where

$$E(\boldsymbol{k}) = E_c + \frac{\hbar^2}{2}\left(\frac{k_x^2}{m_x} + \frac{k_y^2}{m_y} - \frac{k_z^2}{m_z}\right)$$

with positive m_x, m_y, m_z. Show that the density of states can be written near E_c as

$$D(E) \propto \begin{cases} \text{const for } E > E_c \\ D_0 - C(E_c - E)^{1/2} \text{ for } E < E_c \,. \end{cases}$$

Sketch $D(E)$ in the vicinity of (a) a minimum and (b) a saddle point of $E(\boldsymbol{k})$.

7.5 On the basis of the electronic bandstructure and corresponding density of states, explain why copper, in contrast to many other metals, appears colored, i.e., exhibits pronounced spectral structure in its optical constants in the visible spectral range.

7.6 Explain why and how, for diamond and silicon, the energy of the forbidden band E_g changes with increasing temperature.

7.7 Consider an angle resolved UV photoemission spectroscopy (ARUPS) experiment, where UV photons of energy 40.8 eV are incident on the (100) surface of a cubic transition metal with a work function of 4.5 eV. Photoemitted electrons from d-states at 2.2 eV below the Fermi level are detected at an angle of 45° to the surface normal and in the [100] azimuth.

a) Calculate the wave vector $\boldsymbol{k}$ of the emitted electrons.

b) What problem arises in deriving the wave vector $\boldsymbol{k}_i$ of the electronic state from which the electron is released. Consider the components $k_{||}$ and $k_{\perp}$ (parallel and normal to surface) separately.

Panel V
Photoemission Spectroscopy

Experiment

Photoemission electron spectroscopy is the most important experimental method to acquire information on electronic states in solids [V.1]. The possibility to vary energy, incident angle and polarization of the incident photon and to observe kinetic energy and angle of emerging electrons provides means to probe for all occupied electronic states of solids and characterize their properties. Here we focus on experiments concerned with the valence band structure. A typical experimental setup consists of a combination of an energy analyzer and a lens system as shown in Fig. V.1. The sample is mounted on a goniometer that defines the polar and azimuthal angles of electron emission with respect to the surface orientation. Energy analysis is performed with a hemispherical electrostatic deflector. When equipped with corrections for the fringe fields at the entrance and exit apertures by a suitable grading of the aperture potential (Fig. V.1), energy resolutions down to 1 meV can be realized. To keep the resolution constant during energy scans the analyzer operates at constant pass energy while a lens system provides energy retardation or acceleration to match the kinetic energy of photoemitted electrons to the pass energy. The lens system also defines the angular aperture. The combination of exit slit and electron multiplier as shown in Fig. V.1 is frequently

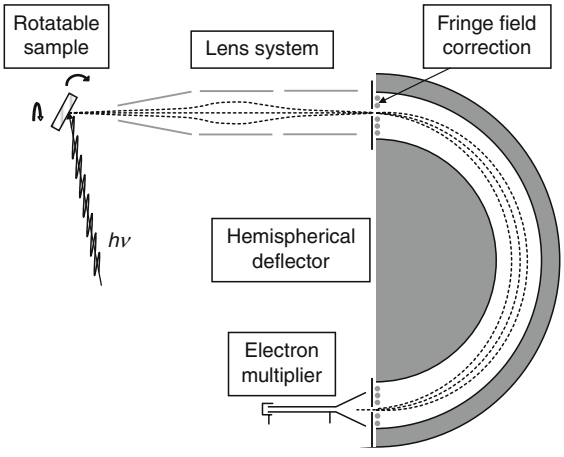

Fig. V.1. Experimental setup for photoemission spectroscopy

replaced by a position-sensitive detector for parallel detection of electrons of different energy. Special analyzers even combine (moderate) energy analysis with a display of emission angles on a position-sensitive detector.

Light Sources

Depending on the photon energy of the light sources, one distinguishes between ***U**ltraviolet **P**hotoemission **S**pectroscopy* (UPS) and ***X**-ray **P**hotoemission **S**pectroscopy* (XPS). The distinction between these two regimes is according to the traditionally available light sources. Ultraviolet radiation is provided by open, differentially pumped gas discharge lamps. Mostly used are the sharp and intense spectral lines of helium at photon energies of 21.22 eV (HeI) and 40.82 eV (HeII). Less common but occasionally also used are neon and argon at 16.85/16.67 eV (NeI), 26.9 eV (NeII), 11.83 eV (ArI) and 13.3/13.48 eV (ArII). Standard laboratory sources for X-rays are the Mg-$K_{\alpha 1,2}$ and Al-$K_{\alpha 1,2}$ emission lines at 1253.6 eV and 1486.6 eV, respectively. The traditional sources have lost some of their importance as synchrotron sources became available for the entire spectral range between 10 eV and several keV. The advantage of synchrotron sources, in particular of undulator beam lines is that they combine high photon fluxes with tunability in a wide spectral range. By varying photon energy and pass energy of the analyzer simultaneously, one can e.g. optimize the cross section for photoemission out of particular electron states and even learn about the unoccupied parts of the band structure. Synchrotron light is polarized, linear-horizontal in the synchrotron plane, left circular and right circular below and above the plane of the ring, respectively, if electrons in the ring circulate clockwise in top view.

The polarization offers additional possibilities. By using selection rules, the symmetry of electron orbitals can be determined with linear polarized light, and with circular polarized light, one can distinguish between spin-up and spin-down states via the effect of magnetic circular dichroism. Fig. V.2 displays the experimental set-up at one of the undulator beam lines (beam line 7) of the ***A**dvanced **L**ight **S**ource* (ALS) at Berkeley, USA [V.2]. With three different gratings, the monochromator covers the photon energy range between 60 and 1200 eV. The resolving power of the monochromator $E/\Delta E$ is about 8000. The energy resolved photon flux is between 10^{12} and 10^{13} s^{-1}. As far as UV-light is concerned these figures of merit are not much better than for the HeI-lamp ($\cong 10^{12}$ photons per second, $\Delta E = 3$ meV, hence $E/\Delta E = 7000$). Thus, the HeI discharge lamp is still competitive in performance, and orders of magnitude lower in operational cost, if a fixed photon energy of 21.2 eV suffices and polarization is not required.

The Photoemission Process

A simple although not exact way of looking upon photoemission is to consider photoemission as a three-step process: Absorption of electromagnetic radiation and the resulting photoexcitation of an electron from an occupied into an

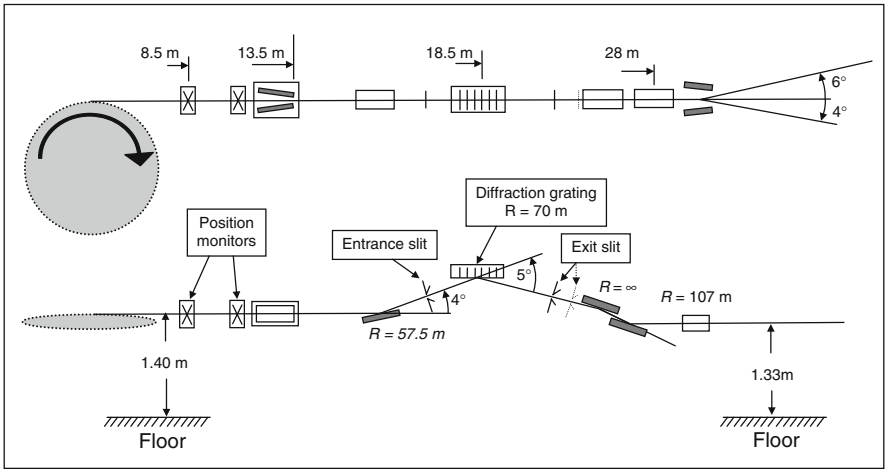

Fig. V.2. The set-up of a the undulator beam line 7 at the ***A****dvanced* ***L****ight* ***S****ource* (ALS) at Berkeley, USA that is commissioned to extended UV-light and soft X-rays. The synchrotron is not drawn to scale. (After Warwick et al. [V.2])

unoccupied state, transport of that electron to the surface, and crossing the potential barrier at the surface (Fig. V.3). In the latter process, the electron looses an a priori unknown amount of momentum perpendicular to the surface, whereby information about the perpendicular component of the wave vector is lost.

The valence band regime is mostly probed with ultraviolet light and occasionally with soft X-ray light. The kinetic energy of photo-excited electrons is therefore between a few eV and about 1-2 keV. The information depth of photoemission spectroscopy in solids is given by the mean free path of those electrons and ranges between 3Å and 30Å depending on the energy. Photoemitted electrons therefore carry information on bulk electronic states as well as on electronic states that are localized to the surface atoms.

The wavelength of photons in the UV-regime amounts to a few hundred Angstroms. All atoms within the information depth therefore experience electromagnetic radiation of nearly the same phase. An alternative way of expressing this fact is that the light contributes nearly no momentum and the transitions between the initial and final electron states $E(\boldsymbol{k})$ are vertical (Fig. V.3a). The photon energy is furthermore outside the regime of collective excitations of the electron gas and outside the regime of extremely strong absorption. The modifications of the electromagnetic field at the surface may then be disregarded. In that case, the absorption of the electromagnetic radiation and therefore the intensity of the photoemission current is proportional to the square of the matrix element of the dipole moment $e\boldsymbol{x}$, i.e. the vector $\boldsymbol{x}^*$ parallel to the electric field with the initial and final

*Most treatments here formulate "momentum operator $\boldsymbol{p}$" which is correct; leads however, save for a factor, to an identical result in the case of a homogeneous electric field.

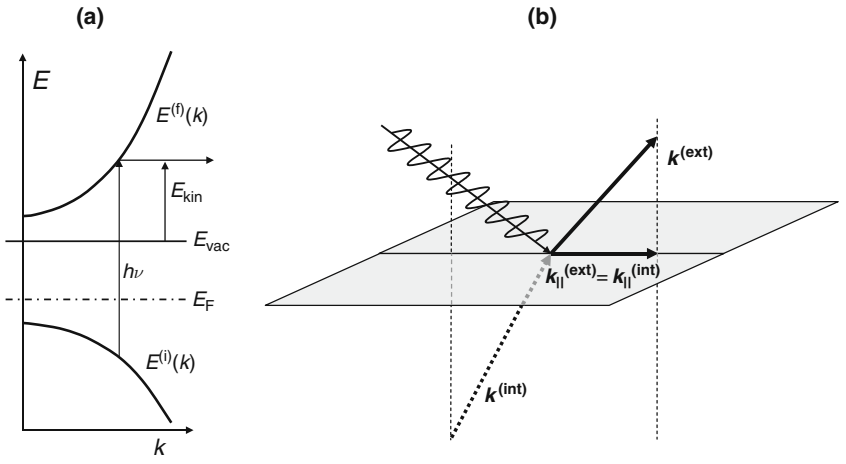

Fig. V.3. Illustration of the photoemission process. (**a**) A photon of energy $h\nu$ excites an electron from the initial state $E^{(\mathrm{i})}(k)$ to the final state $E^{(\mathrm{f})}(k)$ above the vacuum level E_{vac}. The kinetic energy of the photoemitted electron is $E_{\mathrm{kin}} = E^{(\mathrm{f})}(k) - E_{\mathrm{vac}}$. (**b**) The wave vectors of the electron inside $\boldsymbol{k}^{(\mathrm{int})}$ and outside $\boldsymbol{k}^{(\mathrm{ext})}$ have the same parallel components since the spatial phase $i\boldsymbol{r}_{||}\boldsymbol{k}_{||}$ has to be identical to make the wave function continuous at any given point $\boldsymbol{r}_{||}$ of the surface

state (see Sect. 11.10). The current carried by electrons of a particular kinetic energy E_{kin} into a particular direction given by the wave vector $\boldsymbol{k}_{||}^{(\mathrm{el})}$ is proportional to:

$$I_{\mathrm{ph}}(\boldsymbol{k}_{||}^{(\mathrm{el})}, E_{\mathrm{kin}}) \propto \sum_{i,j} \sum_{k_z} \left| \left\langle j, \boldsymbol{k}_{||}, k_z | \boldsymbol{x} | i, \boldsymbol{k}_{||}, k_z \right\rangle \right|^2 \times \delta(E_{\mathrm{kin}} + E_{\mathrm{vac}} - E^{(\mathrm{i})}(\boldsymbol{k}_{||}, k_z) - h\nu)\delta(\boldsymbol{k}_{||} - \boldsymbol{k}_{||}^{(\mathrm{el})}). \tag{V.1}$$

Here, i, j denote the initial and final bands, $\boldsymbol{k}_{||}$, k_z are the components of the wave vector in the initial and the final state, and $E^{(\mathrm{i})}$, E_{vac} are the energies of the initial state and the vacuum level. The matrix element is an integral over the unit surface cell and over the information depth along the z-coordinate. The kinetic energy of the photoemitted electron therefore carries the information on the energy of the initial state by virtue of the energy conservation term in (V.1),

$$E_{\mathrm{kin}} = -E_{\mathrm{vac}} + E^{(\mathrm{i})}(\boldsymbol{k}_{||}, k_z) + h\nu. \tag{V.2}$$

The parallel component of the $\boldsymbol{k}$-vector is conserved for periodic surfaces, as the electron wave function inside has to phase-match to the wave function outside in order to have the wave function continuous at the surface. The $\boldsymbol{k}_{||}$-vector of surface states is therefore fully determined by the $\boldsymbol{k}_{||}$-vector of

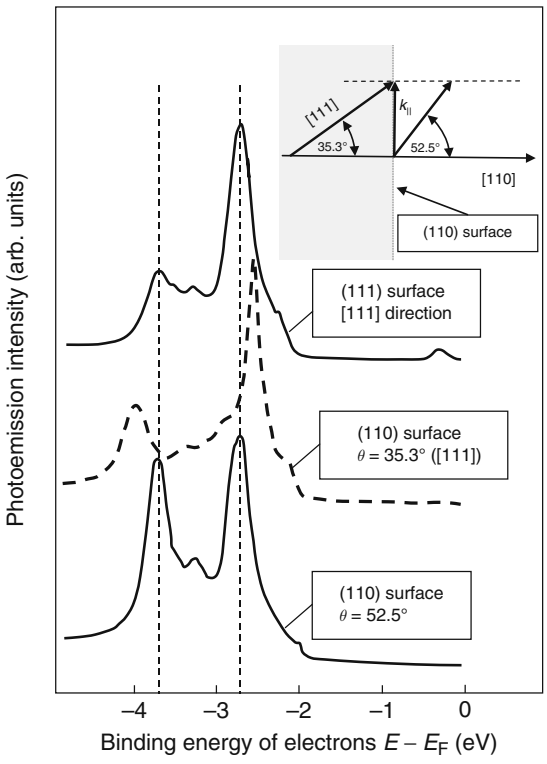

Fig. V.4. Photoemission spectra of Cu(111) and Cu(110) surfaces [V.3] serving to establish the wave vector k_{111} for bulk electronic states: the two prominent peaks appearing in the spectra along [111] on Cu(111) are found at an angle of $\theta = 52.5^\circ$ in the [110] zone on Cu(110). The magnitude of k_{111} is determined by considering $k_{||}$ conservation (V.3). (After Courts and Hüfner [V3])

the photoemitted electron (Fig. V.3b). The vertical component of the $\boldsymbol{k}$-vector of bulk states which is lost in the transgression of the surface potential barrier may be recovered by special techniques.

One technique is triangulation as illustrated with Fig. V.4. A series of photoemission spectra from a Cu(110) surface in the [110] zone as function of angle θ with respect to surface normal is compared to the emission spectrum in the [111] direction on a Cu(111) surface. In the latter case, the internal k vector of the emitting electron states is along [111] because of $\boldsymbol{k}_{||}$ conservation. While on the Cu(110) surface the [111] direction makes an angle of $\theta = 35.2^\circ$ with the surface normal, peaks at the same initial state energies as on Cu(111) are found at $\theta = 52.5^\circ$ (Fig. V.4) because of the refraction of the electrons when they traverse the surface (insert in Fig. V.4). We now calculate the modulus of the $\boldsymbol{k}$ vector of the initial states $k_{111}^{(\mathrm{int})}$ making use of the conservation of the parallel component of the wave vector (Fig. V.3, insert in Fig.V.4):

$$k_{||}^{(\mathrm{int})} = k_{||}^{(\mathrm{ext})} \Rightarrow k_{111}^{(\mathrm{int})} \sin 35^\circ = k^{(\mathrm{ext})} \sin 52.5^\circ. \qquad \text{(V.3)}$$

The moduli of the wave vectors outside $k^{(\mathrm{ext})}$ are calculated from the kinetic energies of the photoemitted electrons. Thus, the peaks observed at –2.7eV and –3.7eV binding energy belong to different k_{111} vectors.

Selection Rules in UPS

The photoemission process obeys certain selection rules that follow from the matrix element in (V.1). Consider for example a surface with a mirror plane. The electron eigenstates belong to either the odd or the even representation. The final state of electrons with trajectories in the mirror plane is even. The matrix element in (V.1) is then nonzero for s-polarized light (polarization in plane of incidence) and even initial electron states and for p-polarized light (polarization perpendicular to the plane of incidence) and odd initial electron states. Hence, by orienting the sample with respect to the polarization plane of the synchrotron light and by observing electrons emitted in the mirror plane one can immediately determine the symmetry of the initial state.

For atomic orbitals with vector character, the p-states, one can furthermore determine the orientation of the orbitals in space from the intensity profile with reference to the polarization of light. Since the vector $\mathbf{x}$ in the matrix elements is oriented as the electric field $\mathscr{E}_0^{(\mathrm{s})}$ of the UV-light at the surface, the photoemission intensity from a p_z-orbital is proportional to $|\mathscr{E}_z^{(\mathrm{s})}|^2$, from a p_x-orbital proportional to $|\mathscr{E}_x^{(\mathrm{s})}|^2$ and from a p_y-orbital proportional to $|\mathscr{E}_y^{(\mathrm{s})}|^2$. By changing the polarization such that either $|\mathscr{E}_x^{(\mathrm{s})}|^2$, $|\mathscr{E}_y^{(\mathrm{s})}|^2$ or $|\mathscr{E}_z^{(\mathrm{s})}|^2$ become zero and looking for the disappearance of the intensity, the orientation of p-orbitals is easily determined.

The flux of electrons that are photoemitted from localized orbitals also shows an interesting dependence on the energy of the final state, which follows directly from the matrix element. If, for example, the initial state is an s-orbital the intensity goes through a minimum when the wavelength of the electron in the final state matches approximately the spatial extension of the initial state since positive and negative contributions to the matrix element cancel. Such minima have been discussed first by J. W. Cooper [V.4] and are therefore named *Cooper minima*.

References

V.1 S. Hüfner: *Photoelectron Spectroscopy*, 2nd ed., Springer series in Solid-State Sci. Vol. 82 (Springer, Berlin, Heidelberg, New York 1996)
H. Lüth: *Solid Surfaces, Interfaces and Thin Films*, 4th. edn., (Springer, Berlin, Heidelberg, New York 2001)
H. Ibach: *Physics of Surfaces and Interfaces* (Springer, Berlin, Heidelberg, New York 2005)

V.2 T. Warwick, P. Heimann, D. Mossessian, W. McKinney, H. Padmore: Rev. Sci. Instr. **66** (1995) 2037

V.3 R. Courts, S. Hüfner: Physics Reports **112**, 55 (1984)

V.4 J. W. Cooper: Phys. Rev. Lett. **13**, 762 (1964)